Tunable flat-band plasmonic quasi-bound states in the continuum based on graphene-assisted metasurfaces

Zhuo Wang,[1] Yue Wang,[1] Zhi Cheng,[1] Jiaqi Qu,[1] Mingjie Cui,[1] Dongmei Huang,[1] and Changyuan Yu[*,1,2]

[1)]*Photonics Research Institute, Department of Electrical and Electronic Engineering, The Hong Kong Polytechnic University, Kowloon, Hong Kong*

[2)]*The Hong Kong Polytechnic University Shenzhen Research Institute, Shenzhen 518057, China*

(*Electronic mail: changyuan.yu@polyu.edu.hk)

(Dated: 4 June 2024)

Bound states in the continuum (BICs) of plasmonic systems offer a powerful method for enhancing light-matter interaction at the nanoscale. The recent emergence of flat-band quasi-BICs has alleviated the limitation of the incident angle of the excitation light on generating high-quality-factor (high-Q-factor) resonances, which makes it feasible to produce substantial near-field enhancement by focused light. However, the current works are limited to passive systems with fixed amplitude and Q-factor, hindering the dynamic tunability of light field enhancement. Here, we design a plasmonic metasurface integrated with monolayer graphene to achieve tunable flat-band quasi-BICs. Under the illumination of tightly focused transverse-magnetic (TM) wave, our simulations show that adjusting the chemical potential of graphene can increase Q-factor from 52.5 to 75.9 and improve absorption amplitude from 81% to 95%. These results pave the way for dynamically adjustable near-field enhancement with tightly focused light.

Bound states in the continuum (BICs) are nonradiative resonant modes overlapped with the spectrum of the radiation continuum. The concept of BICs was first proposed by von Neumann and Wigner in quantum models[1]. It is now considered to be a universal phenomenon in wave systems including photonics[2], plasmonics[3–5], acoustics[6], and optomechanics[7]. When an open system has structural symmetry, the constraints of symmetry can completely decouple resonant modes from all radiation channels. These bound states are classified as symmetry-protected (SP)-BICs[8]. BICs can still exist in systems where symmetry is missing[9]. A well-known example is Friedrich-Wintgen (FW)-BIC which is formed by the interference of resonances belonging to different channels[10]. In addition, a pair of adjacent identical resonances can form BICs by canceling the radiation of each other[11]. The same mechanism can also be applied to a system consisting of a single resonance and its mirror image[12–14]. Theoretically, true BICs can achieve infinite quality-factors (Q-factors) in a boundary-free lossless model. In practice, due to geometric deformation, limited size, and other perturbations, BICs appear as quasi-BICs with finite high Q-factor. Quasi-BICs can be excited by optical beams from far field, and the high-Q characteristic makes quasi-BICs important for generating sharp resonances and realizing ultrahigh near-field enhancement, which paves the way for miniaturized lasers[15–17], ultrasensitive sensing[18,19], and optical modulation[20–22].

High-Q resonances governed by flat-band quasi-BICs have attracted extensive attention in recent years. Ultralow dispersion in the momentum space makes this type of resonance have strong tolerance to light with low spatial coherence. Consequently, high-Q quasi-BICs can be excited by tightly focused light, which fundamentally improves the utilization efficiency of light energy for near-field enhancement. Specifically, a bionic plasmonic metasurface was demonstrated can support surface lattice resonances (SLRs) with ultralow angular dispersion[23]. Under the joint effect of SP-BIC and FW-BIC, the SLRs stimulated by transverse-magnetic (TM) polarized wave can maintain high Q-factors in the range of incident angles from 0° to 60°. Another work employed deep-subwavelength periodic structures to realize polarization insensitive flat-band quasi-BICs[14]. It was found that high-Q (∼71) resonances can be excited by focused light with numerical aperture (NA) of 0.5. In addition, the energy-momentum dispersion relation can be tuned by symmetry breaking[24]. Using band folding effects, flat band-edge quasi-BICs can be adjusted to off-Γ points in the first Brillouin zone[25], which can reduce the damage of angular dispersion on augmented reality (AR) images at large angle oblique incidence. However, in the passive systems mentioned above, the Q-factor and resonant wavelength of the flat-band quasi-BICs cannot be dynamically adjusted, which limits the scope of application.

The combination of two-dimensional (2D) materials and metasurfaces provides a solution for realizing active micro-nano devices[26]. For example, photonic metasurfaces can greatly enhance the second harmonic generation from few-layer GaSe[27] and Transition metal dichalcogenides (TMDs)[28] by BICs mechanism. Besides, utilizing the photoelectric properties of 2D materials, quasi-BICs become adjustable by varying bias voltage[29,30]. However, the responses of those devices are sensitive to the wavevector direction of the incident light, rendering challenges for manipulating focused light.

Here, we proposed a plasmonic metasurface integrated with monolayer graphene to achieve tunable high-Q quasi-BICs for tightly focused TM polarized light. Ultralow average angular dispersion of −0.06 nm/deg was found when the elevation angle (θ) of incidence varies from 0° to 40°. The Q-factor and resonant wavelength of quasi-BICs can be adjusted by changing the chemical potential (μ_c) of graphene. Significant Q-factor improvement (from ∼52.5 to ∼75.9) was found when μ_c increases from 0 eV to 0.6 eV. The designed metasurface demonstrates dynamically adjustable flat-band BICs, promising various potential applications including nanolaser, nonlinear enhancement, and biosensing.

The geometry of the proposed metasurface is shown in Fig.

1a. An array of nano blocks with the same period P in x and y directions is placed on a silica (SiO_2) spacer. The nano block consists of three pieces of elements, they are a middle silicon (Si) layer and two side silver (Ag) layers. The monolayer graphene is in the interface between nano blocks and the spacer layer. The Ag layer at the bottom is mainly for generating specular reflection. The parameters for the design are as follows: $P = 400$ nm, $W = 60$ nm, $L = 160$ nm, $h_1 = 160$ nm, $h_2 = 240$ nm, and $h_3 = 100$ nm. The refractive indices of SiO_2 and Si are modeled by the Sellmeier formula[31] and data obtained by Li[32], respectively. The complex refractive index of Ag is obtained from the experimental results[33].

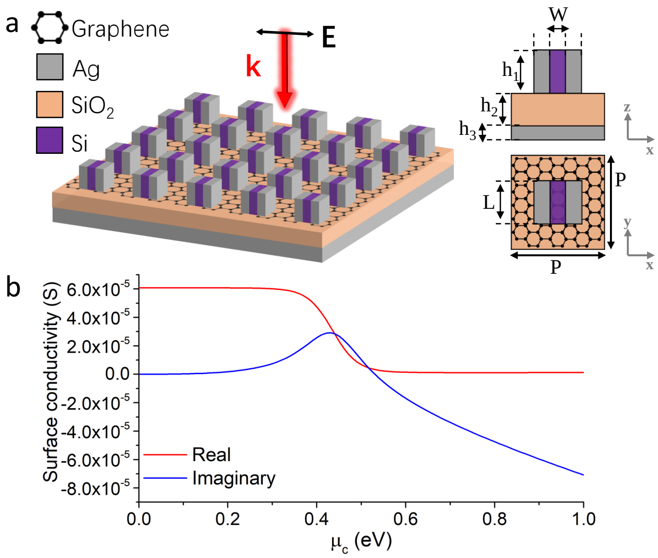

FIG. 1. Schematic of the graphene-assisted metasurface. (a) The metasurface consists of a bottom Ag layer, a middle SiO_2 spacer, and a top nano block array. The monolayer graphene is placed between the spacer and nano block array. The front and top views of a unit cell are illustrated in the right-hand panel. (b) The real part and imaginary part of graphene surface conductivity versus chemical potential μ_c at the wavelength of 1425 nm.

The optical property of monolayer graphene can be described by the Kubo formula[34]

$$\sigma_{\text{intra}} = \frac{-ie^2 k_B T}{\pi\hbar^2(\omega - i2\Gamma)}\left[\frac{\mu_c}{k_B T} + 2\ln\left(\exp\left(\frac{-\mu_c}{k_B T}\right)+1\right)\right], \quad (1)$$

$$\sigma_{\text{inter}} = \frac{-ie^2(\omega - i2\Gamma)}{\pi\hbar^2}\int_0^\infty \frac{f_d(-\xi) - f_d(\xi)}{(\omega - i2\Gamma)^2 - 4(\xi/\hbar)^2}\mathrm{d}\xi, \quad (2)$$

where $f_d(\xi) = (\exp((\xi - \mu_c)/k_B T) + 1)^{-1}$ is Fermi-Dirac distribution, e is the elementary charge, k_B is Boltzmann's constant, $\hbar$ is reduced Planck's constant, and ω is the angular frequency of light. The total surface conductivity σ of graphene is the sum of the intra-band conductivity σ_{intra} and the inter-band conductivity σ_{inter}. At the near-infrared wavelength band, the real part of graphene surface conductivity $\mathrm{Re}(\sigma)$ is dominated by the inter-band transition, which affects the Q-factor of resonant modes. On the other hand, the imaginary part of graphene surface conductivity $\mathrm{Im}(\sigma)$ is determined by the combined effect of inter-band transition and intra-band transition. It will affect the wavelength of the resonant peak. In our simulation, the temperature is $T = 300$ K, and scattering parameter is $\hbar\Gamma = 5$ meV[35,36]. As an example, at the wavelength of 1425 nm, the calculated real part and imaginary part of σ against μ_c are shown in Fig. 1b. When a bias voltage is applied between the graphene and the metal substrate, μ_c can be changed[37], so the metasurface is electrically adjustable.

In the metal-insulator-metal (MIM) nano block, the free current in the metal layers and the displacement current in the insulator can form a closed-loop current[38]. Hence, a magnetic dipole (MD) dominated resonance can be generated. Moreover, the interference between the MD and the light reflected by the Ag substrate can reduce the radiation towards the z direction, which significantly improves the Q-factor of resonance[13,14]. In previous work, it was shown that MD-dominated BICs could be achieved by adjusting the height of the spacer layer[39]. Figure 2a (bottom panel) shows the magnetic field of resonance under the normal incidence of TM polarized wave in the x-y incident plane, a strong MD polarized in the y direction can be found. When the incident angle θ of the TM polarized wave changes (see the top panel of Fig. 2a), the magnetic polarization keeps in the y direction. Therefore, in a wide range of incident angles, the TM polarized wave can effectively excite the MD resonance.

We first used a full-wave solver based on finite element analysis software COMSOL Multiphysics to model the reflectance spectra of the metasurface under the excitation of TM polarized wave at different incident angles. Because monolayer graphene is only a single atomic layer thick ($\sim$ 0.34 nm), in the simulation it can be considered a 2D material with no thickness[40], and its response to the light field can be described by the surface current density as $J = \sigma E$. Figures 2b and 2c show the results in the conditions of $\mu_c = 0$ eV and $\mu_c = 0.6$ eV, respectively. At the incident angle around 70° we can find an accidental BIC, of which the coupling with all radiation channels is inhibited. This accidental BIC can be classified as Fabry-Pérot (FP)-BICs[9], it is formed by the destructive interference between MD-dominated resonance with its mirror image[13]. When θ decreases from the angle of BIC condition, the BIC evolves into quasi-BICs with the increase of spectral linewidth and resonant depth. For both cases of $\mu_c = 0$ eV and $\mu_c = 0.6$ eV, the angular dispersion of the quasi-BICs is very weak, especially in the range from 0° to 40° of θ, the quasi-BICs can maintain a very small resonant wavelength offset (<3 nm) and a large absorption amplitude ($>65\%$). The Q-factors of the excited resonances can be calculated by the formula $Q = \omega_r/\Delta\omega$, where ω_r is the resonant angular frequency and $\Delta\omega$ is the full width of half maximum (FWHM) of the reflectance spectrum. Figure 2d shows the Q-factors of quasi-BICs versus θ under two different graphene chemical potentials. As the incident angle approaches the BIC condition, the Q-factors can be significantly increased due to the reduction of radiative loss. In addition, when μ_c increased from 0 eV to 0.6 eV, the Q-factors of quasi-BICs are effectively boosted by at least 20. From the results in Fig. 1b, we

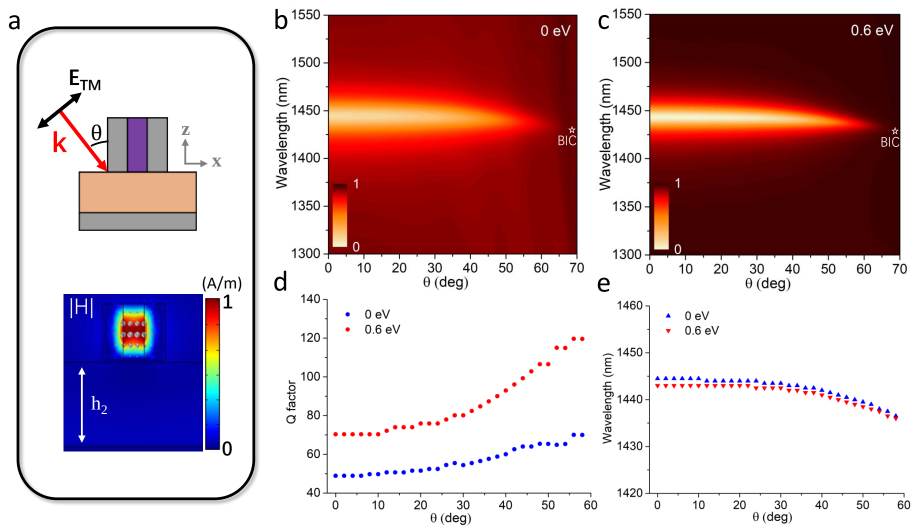

FIG. 2. TM excitation under different incident angles. (a) Schematic of oblique incidence of TM polarized wave in the x-z incident plane (top panel) and magnetic field distribution at the resonant wavelength (bottom panel). (b,c) Reflectance spectra versus incident angle θ when the chemical potential is 0 eV and 0.6 eV, respectively. (d) Calculated Q-factors of resonances according to the reflection spectra. (e) Variation of resonant wavelength with the incident angle.

can find that the real part of σ drops from 6.09×10^{-5} S to almost 0 S when μ_c grows from 0 eV to 0.6 eV, consequently, the dissipative loss of graphene is reduced and the Q-factors of quasi-BICs are improved. Therefore, in the proposed metasurface, the Q-factors of quasi-BICs can be tuned by adjusting the radiative loss and dissipative loss at the same time. Another merit of the design is that the weak angular dispersion characteristic of quasi-BICs is not influenced by the change in graphene surface conductivity. According to the results in Fig. 2e, changing μ_c just leads to a small shift of resonant wavelength, while the property of weak angular dispersion keeps well.

The weak angular dispersion of the metasurface originates from the intrinsic flat-band characteristic of the deep subwavelength periodic structure. We used the eigenfrequency solver of COMSOL Multiphysics to analyze the band structure of the metasurface. In the simulation, the Floquet periodic boundary condition was adopted in the transverse boundaries. The wave vector for Floquet periodicity in the x and y directions are k_x and k_y, respectively. To match the condition that the incident plane is x-z plane, k_y keeps to be zero, and k_x varies from 0 to $0.54\pi/P$. The calculated band structures with different μ_c are shown in Fig. 3a. It can be seen that in all cases the eigenwavelength just decreases by about 2.4 nm when k_x increases from 0 to $0.36\pi/P$. The correspondence between θ and k_x is given by $\theta = \arcsin(k_x/k_r)$, where k_r is the free-space wave vector at the resonant wavelength. It can be obtained that θ is around 40° when $k_x = 0.36\pi/P$. Therefore, the angular dispersion is very low with a value of -0.06 nm/deg. In addition, the resonant wavelength is affected by $\mathrm{Im}(\sigma)$. When μ_c grows from 0 eV to 0.4 eV, the resonant wavelength has a redshift of about 2 nm. After that, continuing to increase μ_c to 0.5 eV and 0.6 eV will cause a blueshift in the resonant wavelength. These results are consistent with the variation trend of $\mathrm{Im}(\sigma)$ in Fig. 1b, which increases first and then decreases. The Q-factor of eigenmodes can be defined by $Q = \mathrm{Re}(\omega_e)/\mathrm{Im}(2\omega_e)$, where $\mathrm{Re}(\omega_e)$ and $\mathrm{Im}(\omega_e)$ are the real and imaginary parts of the eigen angular frequency, respectively. Figure 3b illustrates that the Q-factors grow with the increase of k_x. They reach the maximum around $k_x = 0.53\pi/P$, the equivalent incident angle of which is about 70°. The trend agrees well with the data obtained from the reflectance spectra. In addition, the Q-factors of eigenmodes increase steadily as μ_c grows step by step from 0 eV to 0.6 eV. The reason is that the increase of μ_c reduces the graphene dissipative loss caused by $\mathrm{Re}(\sigma)$. The maximum average improvement of the Q-factors is about 23 when k_x is in the range of $[0, 0.36\pi/P]$. Therefore, the robustness of the high Q-factor and flat band structure makes the metasurface capable to generate tunable high-Q resonances under focused light illumination.

The presence of FP-BIC at oblique incidence can be further demonstrated in the case of eliminating material loss. The imaginary part of the relative permittivity $\mathrm{Im}(\varepsilon_r)$ of Ag is ignored, so Ag is regarded as a perfect conductor. And the real part of the surface conductivity of graphene $\mathrm{Re}(\sigma)$ is set to be zero. In addition, the refractive indexes of all dielectric materials are real. The results are shown in the lower panel of Fig. 3. The eigenwavelengths in Fig. 3c agree well with the results in Fig. 3a, which indicates that the material loss has little influence on the resonant wavelength. In Fig. 3d, because $\mathrm{Re}(\sigma)\equiv0$, the change of μ_c does not affect the Q-factor. We can see that the Q-factors of eigenmodes approach infinity when k_x is about 0.53π/P. The corresponding incident angle is around 70°. This result is consistent with the angle at which the resonant peak disappears in Fig. 2, which provides solid evidence for the existence of BIC.

Next, we analyze the resonances under transverse-electric (TE) polarized wave incidence. As illustrated in Fig. 4a, the

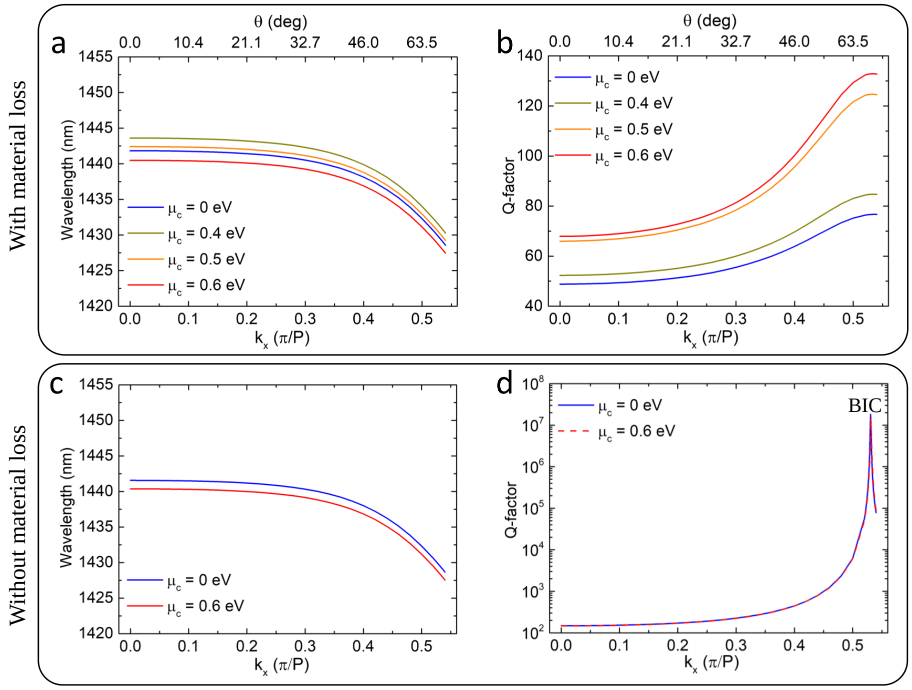

FIG. 3. Eigenmode analysis of metasurface. (a, b) Resonant wavelength and Q-factor of eigenmodes versus x-direction wave vector k_x and the corresponding incident angle θ of TM polarized wave, respectively. (c, d) The results of resonant wavelength and Q-factor, respectively, in the case of ignoring all material loss.

magnetic component of incidence is in the x-z plane. The z-component of magnetic field will increase with θ, hence a z-direction magnetic dipole can be stimulated by oblique incidence. The reflectance spectra when μ_c = 0.6 eV are shown in Fig. 4b. Since the normal incidence cannot excite the z-direction magnetic dipole, no resonant dip appears. With the increase of θ, the resonance depth first increases and then decreases, and the perfect absorption is reached at about 30°. At the same time, the linewidth of the resonance continues to broaden. This is a typical phenomenon of the evolution from BIC to quasi-BIC. Then we calculated the Q-factors of eigenmodes without material loss as shown in Fig. 4e. The Q-factor approaches infinity when $k_x = 0$, which confirms the existence of SP-BIC. The results of eigenwavelength are shown in Fig. 4c. The increase of μ_c from 0 eV to 0.6 eV also causes a blueshift. The decrease of resonant wavelength is about 12 nm when k_x increases from 0 to $0.36\pi/P$. Thus, the corresponding angular dispersion is about -0.3 nm/deg, which is 5 times larger than that of TM incidence. Then, the Q-factors of eigenmodes with material loss are illustrated in Fig. 4d. When k_x is in the range from 0 to $0.2\pi/P$, the Q-factor can be significantly improved by increasing μ_c from 0 eV to 0.6 eV. However, when k_x approaches $0.5\pi/P$, the radiative loss dominates. Consequently, the increase of μ_c can only slightly increase the Q-factor.

By comparing the results of TM incidence and TE incidence, TM incidence has the advantages of vertical excitation and ultraweak angular dispersion, which is more suitable for field enhancement of focused light. To mimic the condition of focused illumination, we calculated the average reflectance spectra ($\bar{R}$) of the TM polarized wave in the x-z incident plane covering the θ from 0° to 40°. The expression is

$$\bar{R}(\lambda) = \frac{1}{N}\sum_{\theta=0^\circ}^{40^\circ} R_\theta^{\mathrm{TM}}(\lambda), \tag{3}$$

where R_θ^{TM} is the reflectance spectrum excited by TM polarized wave at the incident angle θ. N is the number of sampled θ. Here, θ changes from 0° to 40° in steps of 2°, as illustrated schematically by the inset of Fig. 5. Because the real part of graphene surface conductivity can cause dissipative loss, the maximum average reflectance is just ∼0.9 when $\mu_c = 0$ eV. In this case, the Q-factor is relatively low at ∼52.5, and the absorption amplitude is just ∼81%. With the increase of μ_c the dissipation caused by σ decreases, hence the Q-factor increases slightly to 56.6 at $\mu_c = 0.4$ eV. When μ_c is increased to 0.6 eV, the real part of σ becomes close to zero. At this time, the dissipative loss caused by graphene is minimized. Consequently, the Q-factor of the average reflectance spectra increases to ∼75.9. In the meantime, the absorption amplitude grows to ∼95%. The further increase of μ_c from 0.6 eV to 1 eV has little influence on the real part of σ. Instead, the imaginary part of σ is significantly decreased. Therefore, the resonant wavelength decreases by ∼4 nm, while the Q-factor and resonant depth almost do not change. Conventionally, the graphene chemical potential does not exceed 1 eV. The resonant dips of μ_c = 0.4 eV and 1 eV are at 1438.5 nm and 1445.5 nm, respectively. Hence, the controllable spectrum range of flat-band quasi-BICs is about 7 nm. The simulation results demonstrate that the designed metasurface can realize

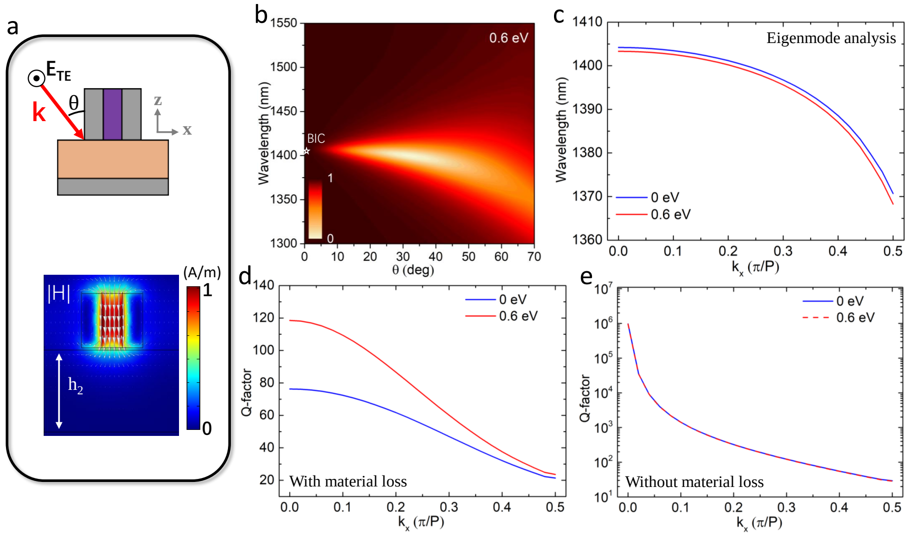

FIG. 4. TE excitation under different incident angle. (a) Schematic of oblique incidence of TE wave in the *x*-*z* incident plane (top panel) and magnetic field distribution at the resonant wavelength (bottom panel). (b) Reflectance spectra versus incident angle θ when the chemical potential is 0.6 eV. (c) Resonant wavelength of eigenmodes versus *x*-direction wavenumber k_x. (d, e) The Q-factors of eigenmodes in the cases with and without material loss, respectively.

dynamically adjustable high-Q flat-band quasi-BICs. It provides a way to regulate the interaction between matter and tightly focused light.

The TM polarized focused light of the *x*-*z* incident plane mentioned above can be generated experimentally[23]. To reduce the undesired spatial components of incidence, the objective needs to be partially blocked by opaque tapes to form a slit along the *x*-direction as shown in the right panel of Fig. 5. The polarization of the focused light can be controlled by tuning the polarization of the collimated light incident to the objective. For example, the *x*-polarized collimated light passing through the modified objective will form a focused TM light. This method enables further experimental testing of the designed metasurface.

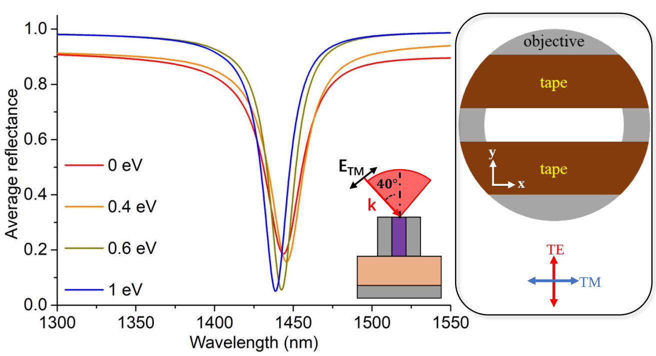

FIG. 5. Average reflectance spectra at different chemical potentials. The inset represents focused TM polarized waves with θ covers from 0° to 40° in the *x*-*z* incident plane illuminate on the metasurface. The right panel illustrates the method of generating the incident light by a partially blocked objective.

The proposed metasurface can be fabricated by a standard cleanroom process, including electron beam lithography (EBL), electron beam deposition, and inductively coupled plasma (ICP) etching. A pioneer work has reported the fabrication of a vertically oriented MIM structure with a 25 nm channel sandwiched between two metal films[41], their processes support the fabrication feasibility of the structures we designed. The fabrication and measurement of the designed metasurface will be carried out in the future.

In this work, we proposed a plasmonic metasurface that can achieve tunable flat-band quasi-BICs by changing the chemical potential of graphene. For the incidence of TM polarized wave, the excited quasi-BICs have ultra-low average angular dispersion (−0.06 nm/deg) in the range of incident angles from 0° to 40°. Furthermore, due to the effect of FP-BICs, the high-Q characteristic of the resonance can be further enhanced at oblique incidence. Thus, light-matter interaction will be improved by tightly focused TM polarized light based on the designed metasurface. More importantly, the flat-band property of quasi-BICs is robust during tuning the surface conductivity of graphene. Instead, the Q-factor is adjustable by changing the dissipative loss of graphene. Consequently, under the illumination of focused TM polarized light with a high NA of ∼0.64, the Q-factor of the stimulated resonance can be improved from ∼52.5 to ∼75.9 by increasing μ_c from 0 eV to over 0.6 eV. Meanwhile, the absorption amplitude grows from ∼81% to ∼95%. This work opens up a way to achieve adjustable flat-band quasi-BICs by combining deep subwavelength metasurfaces with 2D materials, which can be used in the fields of nanolaser, nonlinear enhancement, and biosensing.

ACKNOWLEDGMENTS

The authors gratefully acknowledge Dr. Yao Liang for fruitful discussions. This work is supported by Hong Kong Research Grants Council (GRF Project No. 15209321), by Innovation and Technology Fund (ITS/107/21FP), and by Key Basic Research Scheme of Shenzhen Natural Science Foundation (JCYJ20200109142010888).

[1] J. von Neumann and E. P. Wigner, "Über das Verhalten von Eigenwerten bei adiabatischen Prozessen," The Collected Works of Eugene Paul Wigner: Part A: The Scientific Papers , 294–297 (1993).

[2] D. C. Marinica, A. G. Borisov, and S. V. Shabanov, "Bound States in the Continuum in Photonics," Phys. Rev. Lett. **100**, 183902 (2008).

[3] Y. Liang, K. Koshelev, F. Zhang, H. Lin, S. Lin, J. Wu, B. Jia, and Y. Kivshar, "Bound states in the continuum in anisotropic plasmonic metasurfaces," Nano Letters **20**, 6351–6356 (2020).

[4] A. Aigner, A. Tittl, J. Wang, T. Weber, Y. Kivshar, S. A. Maier, and H. Ren, "Plasmonic bound states in the continuum to tailor light-matter coupling," Science Advances **8**, eadd4816 (2022).

[5] Y. Tang, Y. Liang, J. Yao, M. K. Chen, S. Lin, Z. Wang, J. Zhang, X. G. Huang, C. Yu, and D. P. Tsai, "Chiral bound states in the continuum in plasmonic metasurfaces," Laser & Photonics Reviews , 2200597 (2023).

[6] I. Deriy, I. Toftul, M. Petrov, and A. Bogdanov, "Bound States in the Continuum in Compact Acoustic Resonators," Phys. Rev. Lett. **128**, 084301 (2022).

[7] Y. Yu, X. Xi, and X. Sun, "Observation of mechanical bound states in the continuum in an optomechanical microresonator," Light: Science & Applications **11**, 328 (2022).

[8] K. Koshelev, S. Lepeshov, M. Liu, A. Bogdanov, and Y. Kivshar, "Asymmetric metasurfaces with high-q resonances governed by bound states in the continuum," Phys. Rev. Lett. **121**, 193903 (2018).

[9] C. W. Hsu, B. Zhen, A. D. Stone, J. D. Joannopoulos, and M. Soljačić, "Bound states in the continuum," Nature Reviews Materials **1**, 1–13 (2016).

[10] H. Friedrich and D. Wintgen, "Interfering resonances and bound states in the continuum," Phys. Rev. A **32**, 3231–3242 (1985).

[11] W. Suh, M. F. Yanik, O. Solgaard, and S. Fan, "Displacement-sensitive photonic crystal structures based on guided resonance in photonic crystal slabs," Applied Physics Letters **82**, 1999–2001 (2003).

[12] C. W. Hsu, B. Zhen, S.-L. Chua, S. G. Johnson, J. D. Joannopoulos, and M. Soljačić, "Bloch surface eigenstates within the radiation continuum," Light: Science & Applications **2**, e84–e84 (2013).

[13] G. Yang, S. U. Dev, M. S. Allen, J. W. Allen, and H. Harutyunyan, "Optical bound states in the continuum enabled by magnetic resonances coupled to a mirror," Nano Letters **22**, 2001–2008 (2022).

[14] Z. Wang, Y. Liang, J. Qu, M. K. Chen, M. Cui, Z. Cheng, J. Zhang, J. Yao, S. Chen, D. P. Tsai, and C. Yu, "Plasmonic bound states in the continuum for unpolarized weak spatially coherent light," Photon. Res. **11**, 260–269 (2023).

[15] A. Kodigala, T. Lepetit, Q. Gu, B. Bahari, Y. Fainman, and B. Kanté, "Lasing action from photonic bound states in continuum," Nature **541**, 196–199 (2017).

[16] X. Zhang, Y. Liu, J. Han, Y. Kivshar, and Q. Song, "Chiral emission from resonant metasurfaces," Science **377**, 1215–1218 (2022).

[17] H. Zhong, Y. Yu, Z. Zheng, Z. Ding, X. Zhao, J. Yang, Y. Wei, Y. Chen, and S. Yu, "Ultra-low threshold continuous-wave quantum dot mini-BIC lasers," Light: Science & Applications **12**, 100 (2023).

[18] W. Suh, O. Solgaard, and S. Fan, "Displacement sensing using evanescent tunneling between guided resonances in photonic crystal slabs," Journal of Applied Physics **98**, 033102 (2005).

[19] S. Romano, G. Zito, S. Torino, G. Calafiore, E. Penzo, G. Coppola, S. Cabrini, I. Rendina, and V. Mocella, "Label-free sensing of ultralow-weight molecules with all-dielectric metasurfaces supporting bound states in the continuum," Photon. Res. **6**, 726–733 (2018).

[20] Z. Yu and X. Sun, "Acousto-optic modulation of photonic bound state in the continuum," Light: Science & Applications **9**, 1 (2020).

[21] M. M. Salary and H. Mosallaei, "Tunable all-dielectric metasurfaces for phase-only modulation of transmitted light based on quasi-bound states in the continuum," ACS Photonics **7**, 1813–1829 (2020).

[22] X. Sun, J. Sun, Z. Wang, L. Wang, F. Qiu, and L. Wen, "Manipulating dual bound states in the continuum for efficient spatial light modulator," Nano Letters (2022).

[23] Y. Liang, H. Lin, S. Lin, J. Wu, W. Li, F. Meng, Y. Yang, X. Huang, B. Jia, and Y. Kivshar, "Hybrid anisotropic plasmonic metasurfaces with multiple resonances of focused light beams," Nano Letters **21**, 8917–8923 (2021).

[24] H. S. Nguyen, F. Dubois, T. Deschamps, S. Cueff, A. Pardon, J.-L. Leclercq, C. Seassal, X. Letartre, and P. Viktorovitch, "Symmetry Breaking in Photonic Crystals: On-Demand Dispersion from Flatband to Dirac Cones," Phys. Rev. Lett. **120**, 066102 (2018).

[25] A. C. Overvig, M. Cotrufo, M. Markowitz, Y. Zhou, B. Hao, K. Stensvad, C. Schardt, and A. Alù, "Zone-Folded Quasi-bound State Metasurfaces with Customized, Symmetry-Protected Energy-Momentum Relations," ACS Photonics (2023).

[26] A. Elbanna, H. Jiang, Q. Fu, J.-F. Zhu, Y. Liu, M. Zhao, D. Liu, S. Lai, X. W. Chua, J. Pan, Z. X. Shen, L. Wu, Z. Liu, C.-W. Qiu, and J. Teng, "2D Material Infrared Photonics and Plasmonics," ACS Nano **17**, 4134–4179 (2023), pMID: 36821785.

[27] Z. Liu, J. Wang, B. Chen, Y. Wei, W. Liu, and J. Liu, "Giant Enhancement of Continuous Wave Second Harmonic Generation from Few-Layer GaSe Coupled to High-Q Quasi Bound States in the Continuum," Nano Letters **21**, 7405–7410 (2021), pMID: 34232665.

[28] P. Hong, L. Xu, and M. Rahmani, "Dual bound states in the continuum enhanced second harmonic generation with transition metal dichalcogenides monolayer," Opto-Electron Adv **5**, 200097–1–200097–8 (2022).

[29] C. Zhao, W. Chen, J. Wei, W. Deng, Y. Yan, Y. Zhang, and C.-W. Qiu, "Electrically tunable and robust bound states in the continuum enabled by 2d transition metal dichalcogenide," Advanced Optical Materials **10**, 2201634 (2022).

[30] S. Xiao, X. Wang, J. Duan, T. Liu, and T. Yu, "Engineering light absorption at critical coupling via bound states in the continuum," J. Opt. Soc. Am. B **38**, 1325–1330 (2021).

[31] I. H. Malitson, "Interspecimen comparison of the refractive index of fused silica∗,†," J. Opt. Soc. Am. **55**, 1205–1209 (1965).

[32] H. H. Li, "Refractive index of silicon and germanium and its wavelength and temperature derivatives," Journal of Physical and Chemical Reference Data **9**, 561–658 (1980), https://pubs.aip.org/aip/jpr/article-pdf/9/3/561/8184276/561_1_online.pdf.

[33] P. B. Johnson and R. W. Christy, "Optical constants of the noble metals," Phys. Rev. B **6**, 4370–4379 (1972).

[34] G. W. Hanson, "Dyadic Green's functions and guided surface waves for a surface conductivity model of graphene," Journal of Applied Physics **103**, 064302 (2008).

[35] A. B. Kuzmenko, E. van Heumen, F. Carbone, and D. van der Marel, "Universal optical conductance of graphite," Phys. Rev. Lett. **100**, 117401 (2008).

[36] F. Xu, S. Das, Y. Gong, Q. Liu, H.-C. Chien, H.-Y. Chiu, J. Wu, and R. Hui, "Complex refractive index tunability of graphene at 1550 nm wavelength," Applied Physics Letters **106**, 031109 (2015).

[37] Y. Yao, R. Shankar, M. A. Kats, Y. Song, J. Kong, M. Loncar, and F. Capasso, "Electrically Tunable Metasurface Perfect Absorbers for Ultrathin Mid-Infrared Optical Modulators," Nano Letters **14**, 6526–6532 (2014).

[38] Y. Zhang, P. Yue, J.-Y. Liu, W. Geng, Y.-T. Bai, and S.-D. Liu, "Ideal magnetic dipole resonances with metal-dielectric-metal hybridized nanodisks," Opt. Express **27**, 16143–16155 (2019).

[39] Z. Wang, Y. Liang, M. Cui, J. Qu, Z. Cheng, and C. Yu, "Bound states in the continuum in plasmonic metasurfaces for enhancing graphene-assisted light modulation," in *TENCON 2022 - 2022 IEEE Region 10 Conference (TENCON)* (2022) pp. 1–3.

[40] D. Wang, N. K. Emani, T.-F. Chung, L. J. Prokopeva, A. V. Kildishev, V. M. Shalaev, Y. P. Chen, and A. Boltasseva, "Plasmon resonance in single- and double-layer CVD graphene nanoribbons," in *2015 Conference on Lasers and Electro-Optics (CLEO)* (2015) pp. 1–2.

[41] D.-S. Su, D. P. Tsai, T.-J. Yen, and T. Tanaka, "Ultrasensitive and Selective Gas Sensor Based on a Channel Plasmonic Structure with an Enormous Hot Spot Region," ACS Sensors **4**, 2900–2907 (2019).